Available online at www.sciencedirect.com
SCIENCE DIRECT®
Journal of Solid State Chemistry 176 (2003) 556–566
JOURNAL OF SOLID STATE CHEMISTRY
http://elsevier.com/locate/jssc

A DFT study of lithium battery materials: application to the β-$VOXO_4$ systems (X = P, As, S)

Maxence Launay, Florent Boucher,* Pascal Gressier, and Guy Ouvrard

Laboratoire de Chimie des Solides, Institut des Matériaux Jean Rouxel, UMR 6502 CNRS-Université de Nantes, 2 rue de la Houssinière, BP 32229, 44322 Nantes Cedex 3, France

Received 12 February 2003; received in revised form 23 May 2003; accepted 5 June 2003

Abstract

$VOXO_4$ systems have been considered as potential lithium battery electrodes. They mainly present two distinct structural types: the tetragonal "α" type with a two-dimensional framework, and the three-dimensional orthorhombic "β". DFT calculations were performed on this latter system for several β-Li_xVOXO_4 compounds ($x = 0, 1$; X = P, As, S). They allowed to propose structural models for $VOAsO_4$ and $LiVOSO_4$, not fully crystallographically well described yet. Based on an experimental model of two-phase processes, these calculations led also to a good simulation of electrochemical potential values. A density of states analysis put in evidence the "inductive effect" and the role played by $(XO_4)^{n-}$ groups inside the host frameworks on these potentials.

Keywords: β-$VOXO_4$; Lithium battery; Structure optimizations; Potential calculations; Inductive effect

1. Introduction

During the last 10 years, vanadium compounds used as positives in lithium batteries have been widely investigated from both experimental and theoretical points of view [1–14]. Since vanadium offers a quite large range of oxidation states (from II to V), various amounts of lithium can be intercalated, giving high and useful electrochemical potentials. Some examples of potential range and oxidation states in such vanadium compounds are given in Table 1.

Many research works on the $Li_xV_2O_5$ systems have been undertaken [1,2], and have shown the existence of three different systems, labeled "α", "γ" and "ω", each one having a specific electrochemical behavior. For example, α-V_2O_5 successively transforms into ε-$Li_{0.5}V_2O_5$, δ-$Li_1V_2O_5$, ζ-$Li_2V_2O_5$ and finally ω-$Li_3V_2O_5$. Each step corresponds to more or less important structural rearrangements of the VO_5 polyhedra in the host structure. In the whole intercalation range of α-V_2O_5, the potential varies from 3.6 to 2.0 V. Based on these experimental observations, few theoretical approaches have been done in order to better understand the properties of the $Li_xV_2O_5$ systems [3–5]. In the later study, the authors succeeded both in an accurate simulation of the electrochemical potential and in a precise structural description of the ω-$Li_3V_2O_5$ phase [5].

In the same period, research works were devoted to some vanadium compounds having a Nasicon-like structure [6–12]. These phases were discovered more than 30 years ago: Nasicon stands for "NAtrium Super Ionic CONductors" [15,16]. They present many "lantern" $M_2X_3O_{18}$ units in the cell (M: transition metal; X: mainly P or S). These lanterns are made of three XO_4 tetrahedra linked to two MO_6 octahedra (one up, one down). They are differently connected, depending on the structure. In the rhombohedral structure, lanterns develop along the three-fold **c**-axis, while in the monoclinic one, lantern patterns follow two different directions. In all structures, there are many crystallographic sites available for the alkaline "A" intercalation, explaining the high ionic conductivity of these materials. Some vanadium derivatives, as $Li_xV_2(SO_4)_3$ ($0 \leqslant x \leqslant 2$) or $Li_xV_2(PO_4)_3$ ($1 \leqslant x \leqslant 3$), present quite high potentials [17] (Table 1). Morgan et al. have performed computational studies on a wide range of Nasicon materials with the $Li_xM_2(PO_4)_3$ formulation (M = Ti, V, Cr, Mn, Fe, Co, Ni, Nb) in order to improve the understanding of the

*Corresponding author. Fax: +33-2-40-37-39-95.
E-mail addresses: maxence.launay@cnrs-imn.fr (M. Launay), florent.boucher@cnrs-imn.fr (F. Boucher).

0022-4596/03/$ - see front matter © 2003 Elsevier Inc. All rights reserved.
doi:10.1016/S0022-4596(03)00331-1

Table 1
Experimental voltages and oxidation states for some vanadium containing lithium battery materials

$Li_xV_2O_5$ [5]	Li_xVOPO_4 [30]	Li_xVOSO_4 [32]	$Li_xV_2(PO_4)_3$ [17]	$Li_xV_2(SO_4)_3$ [17]
$0 \leqslant x \leqslant 2$	$0 \leqslant x \leqslant 1$	$0 \leqslant x \leqslant 1$	$1 \leqslant x \leqslant 3$	$0 \leqslant x \leqslant 2$
V^V/V^{IV}	V^V/V^{IV}	V^{IV}/V^{III}	V^{IV}/V^{III}	V^{III}/V^{II}
2.90 V	3.98 V	2.84 V	3.80 V	2.50 V

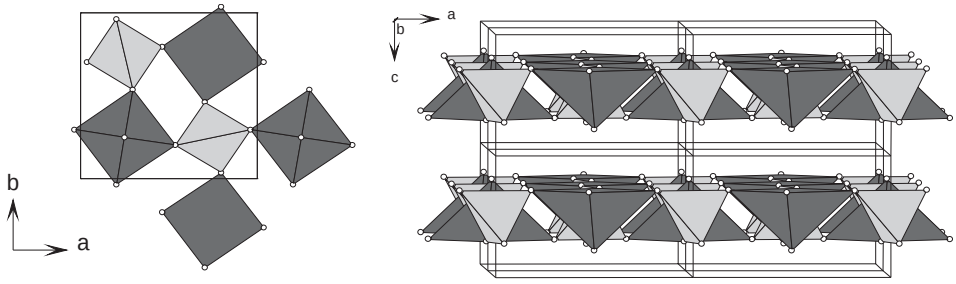

Fig. 1. Schematic representation of the α-$VOXO_4$ structure. Left: view along the tetragonal axis, each $(XO_4)^{n-}$ group (light grey) is connected to four different VO_5 square pyramids (dark grey). Right: perspective view putting in evidence the 2D character.

experimental results [18]. They were able to reproduce with a good accuracy the voltage of the known systems. They have also predicted the electrochemical potentials of many new compounds.

Compounds with $VOXO_4$ ($X = P, S, As$) formula are structurally intermediate between pure oxides and Nasicon-like materials. Thus, whereas the oxygen atoms of VO_5 polyhedra are all connected to XO_4 groups in Nasicon frameworks, some of them are only bound to V atoms in $VOXO_4$ structures, as in the V_2O_5 case. Table 1 shows that the electrochemical behavior of the $VOXO_4$ compounds is also intermediate between oxides and Nasicon-like materials. Such a behavior can be explained by the "inductive effect", which was first mentioned by Manthiram and Goodenough for the $Li_xFe_2(XO_4)_3$ systems with $X = Mo$ and W [19].

The first aim of this study is to reproduce from first-principle calculations the experimental electrochemical potentials in the $VOXO_4$ family. This is done via structure optimizations associated with total energy calculations. In a second step, an analysis of the band structure by comparison of the density of states (DOS) will be presented, in order to precise the role played by the $(XO_4)^{n-}$ groups, namely the inductive effect. Finally, we will present a simple model that allows an interpretation of the electrochemical potentials using the calculated band structures.

2. Experimental background

2.1. Structural description

Compounds with an A_xMOXO_4, nH_2O formula are known since more than 20 years [20–26]. In these compounds, A can be an alkaline element (Li, Na, K) [27], M is a transition metal (Ti, V, Nb, Mo and Ta), and X another element: Si, P, S, Ge or As. For safety reasons, these hydrated compounds still set an experimental problem, since water is unwanted in batteries materials. That is the reason why we will focus here on the dehydrated structures (i.e. $n = 0$), the only compounds of interest from electrochemical and industrial points of view. Moreover, we will restrict our study to the cases where A is Li and M is vanadium. The choice of vanadium reduces the problems that usually occur with the density functional theory (DFT) concerning the treatment of the electronic correlation for d electrons.

For the Li_xVOXO_4 materials, two structural types, called "α" and "β", are reported in the literature. The α compounds are described in a tetragonal symmetry (space group $P4/n$ (#85)) and the cell parameters are: $\mathbf{a} = \mathbf{b} \approx 6.0$ Å and $\mathbf{c} \approx 4.5$ Å [21]. All the quite regular XO_4 tetrahedra are connected in the (**a**, **b**) plane to four different VO_5 square pyramids. The tops of these VO_5 square pyramids are alternatively directed towards "up" and "down" directions of the **c**-axis (Fig. 1). These compounds show a lamellar character (2D materials) (right part of Fig. 1), like α- and γ-V_2O_5; this explains the easy hydration of these materials [24]. A 2D–3D transformation is expected for the low oxidation states of vanadium with the occurrence of V–O bonds through the gap associated to the transformation of square pyramids into octahedra (*vide infra*).

When there is no distortion, the β compounds adopt an orthorhombic structure: the space group is *Pnma* (#62) and corresponding cell parameters are roughly: $\mathbf{a} \approx 7$–8 Å, $\mathbf{b} \approx 6$–6.5 Å and $\mathbf{c} \approx 7$–7.5 Å [20]. The structure can be described from a succession of square

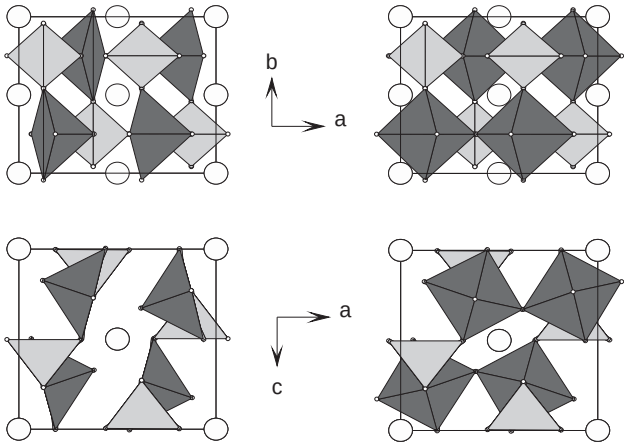

Fig. 2. Schematic representation of the β-Li_xVOXO_4 structure, with XO_4 in light grey, VO_5 or VO_6 in dark grey, and lithium atoms in large open circles. Left: the case of a V^V or V^{IV} with square pyramids. Right: the case of a V^{III} or V^{II} with distorted octahedra. Up: projection along the **c**-axis to show the existence of $[VO_5]_\infty$ alignments along the **a** direction. Down: projection along the **b**-axis to show the interconnections between the alignments via the XO_4 tetrahedra.

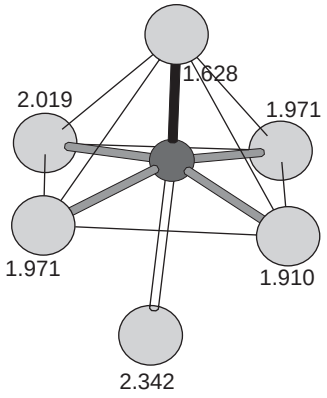

Fig. 3. First vanadium coordination shell in β-$LiVOPO_4$ (all distances are given in Å). The short vanadyl bond is represented in black; the longest V–O bond (in white) is quite too long to consider a VO_6 octahedron.

pyramids developed in the **a** direction (left part of Fig. 2). For low-oxidation states of vanadium, they are changed into distorted octahedra sharing corners in the same direction (right part of Fig. 2). Each XO_4 group is connected to two VO_n polyhedra of a same chain, while the other two corners are connected to two different chains. The XO_4–VO_n–XO_4 succession thus occurs along the **b**-axis. This structural arrangement gives a 3D character to the β-like structures.

As explained above, either square pyramids or distorted octahedra may be considered in all $VOXO_4$ structures. When vanadium is at the oxidation state of V or IV, a short V–O distance, lower than 1.8 Å, is observed. In the opposite direction of this "vanadyl" bond, a long V–O distance, larger than 2.2 Å, is found. The corresponding coordination is often considered as a square pyramid. Within a pyramid, the vanadium atom is shifted away from the center of the square plane (Fig. 3) (more details about the common vanadium environments can be found in [27–29]). For lower oxidation states, the vanadyl bond is not observed and a more symmetrical environment is found. Polyhedra can then be seen as octahedra even if they are often distorted.

2.2. Electrochemical behavior

The voltage curves show only one plateau, which may be attributed to a two-phase process for the lithium intercalation [30–32]. The α and β types of structures contain the same XO_4 and VO_5 polyhedra, but there is less information in the literature about the α-Li_xVOXO_4 structures (with $x = 0$ or 1) for the same X atom. Therefore, we focus our study on the six following β type compounds, forming three couples of materials: first $VOPO_4$–$LiVOPO_4$ [30], then $VOAsO_4$–$LiVOAsO_4$ [31], and finally $VOSO_4$–$LiVOSO_4$ [32].

From X-ray diffraction studies, it has been concluded that, during the lithiation process, alkaline atoms enter the only available octahedral site in the β host framework. The lithium is found in the special position 4a of the *Pnma* space group.

3. Computational details

3.1. Structure optimizations and total energy calculations

Our calculations for the optimizations of Li_xVOXO_4 structures (where $x = 0$ or 1 and X = P, As, S) have been performed by using the Vienna Ab initio Simulation Program (VASP) [33–36], a package based on the density functional theory. The wave functions are expanded in a plane-wave basis set with kinetic energy below 700 eV (from 14 000 up to 16 000 plane waves are necessary, i.e. about 500 plane waves per atom). The VASP package is used with the projector augmented wave (PAW) method of Blöchl [37,38]; in a general way, PAW are expected to be more accurate than the Vanderbilt ultra-soft pseudo-potentials [39] to describe the ion–electron interaction, because they provide an exact valence wave function in the core region of the electron orbitals. The electronic exchange and correlation are treated in the local density approximation (LDA) and corrections are taken into account by the generalized gradient approximation (GGA) exchange and correlation functional of Perdew-Wang [40,41]. The integration in the Brillouin zone is done by using the tetrahedron method corrected by Blöchl [42] on a set of **k**-points ($3 \times 4 \times 3$) determined by the Monkhorst–Pack scheme (12 irreducible **k**-points) [43]. All the optimizations of atomic coordinates and cell parameters are

driven by following a conjugate gradient minimization of the total energy scheme (Hellmann-Feynman forces on the atoms and stresses on the unit cell [44]). A convergence of the total energy close to 10 meV per formula unit (FU) is achieved with such parameters, and no significant change in the total energy and charge density is obtained by using a larger set of **k**-points.

For calculations of total energies and potentials we have used the optimized structures instead of the experimental ones for two reasons. First, it allows to validate the parameters used for calculations: accuracy of projectors, completeness of plane wave basis sets, density of **k**-points sets and quality of the exchange correlation potential. Second, it also guarantees that the DFT variational principle is respected: finding the optimum electronic density that leads to the ground state total energy. All the structure optimizations are done with the same procedure. In a first step, the initial structure is generated considering either the crystallographically known structures for four of the six studied compounds [20,22,31,45] or hypothetical ones for the two others: $LiVOSO_4$ and $VOAsO_4$. For $VOAsO_4$, while the structure is still unknown, the cell parameters have been already determined [31]. Thereafter, we simultaneously perform an optimization of all atomic positions and unit cell parameters. The initial given space group symmetry is kept during this step in order to reduce the computing time. Finally, a specific calculation is performed in order to obtain an accurate value of the total energy for the relaxed system. In the case of a d^1 or d^2 electronic configuration for the vanadium ($LiVOPO_4$, $LiVOAsO_4$, $VOSO_4$, $LiVOSO_4$), two types of calculations are considered, without and with spin polarization. An antiferromagnetic (AF) ordering along the **a**-axis is introduced in agreement with the experimental data [31,46]. All calculations are performed within the approximation of ideal materials having exact stoichiometric formulas.

3.2. Band structure calculations

All band structures calculations have been performed by using the WIEN2K code [47,48], a program based on the density functional theory (DFT) and using the full potential linearized plane wave (FLAPW) method [49]. In this case, the previously optimized structures are introduced and the same exchange and correlation potential is used. The values of spheres radii of Li, V, P, As, S and O atoms are, respectively, taken equal to 1.70, 1.60, 1.45, 1.75, 1.40 and 1.40 a.u. The $R_{MT}K_{max}$ parameter, which is the product of the smallest muffin-tin radius by the plane wave cut-off, is fixed to 7. About 5000 to 5700 plane waves for Li_xVOXO_4 ($x = 0, 1$; $X =$ P, As, S) compounds are used to expand the wave function. Self-consistent cycles are run on about 36 **k**-points, i.e. from 8 to 10 **k**-points within the irreducible part of the Brillouin zone. When necessary, a spin polarization is introduced.

4. Geometry optimizations: results and discussion

The optimized cell parameters for the Li_xVOXO_4 systems (except $LiVOSO_4$, discussed later on) are given in Table 2 for both non-spin-polarized (NSP) and spin-polarized (SP) calculations. From a comparison with the experimental values, it may be concluded that our VASP/PAW calculations allow a correct prediction of the cell parameters with a general tendency to overestimate the cell volume. This behavior is generally

Table 2
Comparison of the experimental and optimized[a] cell parameters for the β-Li_xVOXO_4 family

	$VOPO_4$ [20]	$VOAsO_4$ [31]	$VOSO_4$ [22]	$LiVOPO_4$ [45]	$LiVOAsO_4$ [31]
Exp.					
a (Å)	7.770(3)	7.922(2)	7.376(3)	7.444(2)	7.5916(2)
b (Å)	6.143(3)	6.316(2)	6.269(3)	6.300(1)	6.4713(2)
c (Å)	6.965(3)	7.194(2)	7.082(3)	7.174(2)	7.4216(2)
V (Å^3)	332.45(25)	359.95(20)	327.47(25)	336.44(14)	364.60(20)
NSP					
a (Å)	7.778 (+0.1%)	7.909 (−0.2%)	7.222 (−2.1%)	7.420 (−0.3%)	7.539 (−0.7%)
b (Å)	6.172 (+0.5%)	6.409 (+1.5%)	6.309 (+0.6%)	6.314 (+0.2%)	6.504 (+0.5%)
c (Å)	7.084 (+1.7%)	7.506 (+4.3%)	7.222 (+2.0%)	7.237 (+0.9%)	7.573 (+2.0%)
V (Å^3)	340.1 (+2.3%)	380.4 (+5.7%)	329.0 (+0.5%)	339.0 (+0.8%)	371.3 (+1.8%)
SP					
a (Å)			7.286 (−1.2%)	7.463 (+0.3%)	7.591 (−0.0%)
b (Å)			6.299 (+0.5%)	6.315 (+0.2%)	6.534 (+1.0%)
c (Å)			7.190 (+1.5%)	7.221 (+0.7%)	7.492 (+0.9%)
V (Å^3)			330.0 (+0.8%)	340.3 (+1.2%)	371.7 (+2.0%)

[a] Discrepancies between the values are given in parentheses. NSP and SP mean non-spin-polarized and spin-polarized calculations, respectively.

observed when GGA exchange and correlation potentials are used. We may notice that the cell parameters do not behave identically. The **a** parameters are very close to the experimental values, while larger discrepancies are observed for the **c** parameter. In order to interpret these different behaviors, we may consider the evolution of the bond lengths (Table 3). The mean X–O bond lengths are generally overestimated and the mean V–O and Li–O bond lengths are correct. However, for the V–O distances, a systematic overestimation of the shortest V–O (vanadyl) bond is observed and the longest one is underestimated by the same amount. Thus, the off-centering of the vanadium atom in the square pyramid is reduced. As the V–O distances in the square plane of the pyramids are constant, this vanadium displacement induces an expansion of the equatorial O–O distances. This effect, coupled with the overestimation of the X–O bonds, explains the overestimation of the **b** and **c** parameters. The good values obtained for **a** parameters are consistent with the similar lengthening and shortening of the axial V–O bonds. Finally, it should be noticed that SP calculations lead to bond lengths which are closer to the experimental values than those obtained from NSP calculations.

In order to validate the results for the unknown structures ($VOAsO_4$ and $LiVOSO_4$), Brown valence calculations have been performed [50]. Bond valence methods are semi-empirical ways to correlate the anion–cation bond lengths in the structure with the coordination number of the studied cation. Historically, Goldschmidt [51] and Pauling [52,53] correlated bond lengths and bond orders. In the present work, we use the Zachariasen [54] relation: $V = \sum_i \exp[-(R_i - d)/B]$. In this equation, V, R_i and d, respectively, refer to the cation valence, the individual anion–cation bond length, and the length of the same bond which has a valence equal to 1; $B = 0.37$ [55] is known as the bond softness parameter, and is empirically determined. Calculated vanadium valences for SP optimized structures with the "d" parameters of Brese and O'Keeffe [56] are given in Table 4. These values are in good agreement with the formal oxidation states, with noticeable discrepancies for the X cations in agreement with the overestimated X–O distances. In the case of $VOAsO_4$ and $LiVOSO_4$ (*vide infra*), this agreement allows to conclude that the proposed structures are reliable.

Table 3
List of bond lengths (in Angstroms) for the experimental and optimized[a] structures of the β-Li_xVOXO_4 compounds

	$V–O_{min}$	$V–O_{max}$	⟨V–O⟩	⟨X–O⟩	⟨Li–O⟩
$VOPO_4$ exp.	1.565(7)	2.591(7)	1.947(7)	1.528(6)	
$VOPO_4$ NSP	1.601	2.552	1.954	1.544	
$VOAsO_4$ NSP	1.604	2.539	1.955	1.707	
$VOSO_4$ exp.	1.598(2)	2.270(2)	1.975(2)	1.468(2)	
$VOSO_4$ NSP	1.651	2.096	1.954	1.485	
$VOSO_4$ SP	1.637	2.173	1.966	1.486	
$LiVOPO_4$ exp.	1.628(3)	2.342(3)	1.973(3)	1.534(3)	2.113(2)
$LiVOPO_4$ NSP	1.670	2.308	1.969	1.548	2.111
$LiVOPO_4$ SP	1.666	2.329	1.976	1.550	2.110
$LiVOAsO_4$ exp.	1.633(6)	2.369(6)	1.981(6)	1.695(5)	2.126(4)
$LiVOAsO_4$ NSP	1.670	2.269	1.966	1.725	2.142
$LiVOAsO_4$ SP	1.664	2.308	1.982	1.715	2.135

[a] NSP and SP mean non-spin-polarized and spin-polarized calculations, respectively.

4.1. *The* $LiVOSO_4$ *structure optimization*

$LiVOSO_4$ is not a crystallographically well-known compound yet, as only a few studies have been reported on this intercalated system [57]. The main problem in this system is that the environment of the vanadium atoms changes from square pyramids to distorted octahedra during the lithiation, while the vanadium oxidation state goes from IV to III [28]. A strong modification of the unit cell is expected. Two different calculations have been performed according to two different models. The first one refers to a topotactic reaction, which considers that the $LiVOSO_4$ unit cell is quite similar to those with phosphorus or arsenic. The second one implies a monoclinic ($P2_1/a$) distortion, with a doubling of the **a** parameter (parallel to the $[VO_5]_\infty$ chains). Such a distortion has been suggested by experimental results [57].

In the orthorhombic case, the cell parameters after a SP optimization are consistent with those expected for a lithium intercalation in $VOSO_4$. As for Li_xVOPO_4 and Li_xVOAsO_4 systems, we got a shortening of the cell parameter along the chains from $\mathbf{a} = 7.286$ Å for $VOSO_4$ to $\mathbf{a} = 7.108$ Å for $LiVOSO_4$, and an increasing of the two others: **b** parameter from 6.299 to 6.519 Å and **c** parameter from 7.190 to 7.454 Å. Also, the calculated interatomic distances induce rather good calculated bond valences: $Li^{I} = 0.94$ and $V^{III} = 2.96$. These results tend to prove that the structure could be a

Table 4
Results of bond valence calculations performed on the optimized structures of the β-$VOXO_4$ compounds

	$V^{V}OPO_4$	$LiV^{IV}OPO_4$	$V^{V}OAsO_4$	$LiV^{IV}OAsO_4$	$V^{IV}OSO_4$	$LiV^{III}OSO_4$
Li		1.06		1.03		0.94
V	5.00	4.08	4.96	4.00	4.09	2.96
X	4.71	4.63	4.70	4.60	5.81	5.79

classical β model. However, considering the proposed monoclinic distorted unit cell (space group $P2_1/a$, $\mathbf{a}' = 2\mathbf{a}$), a distortion remains after a SP optimization with the following cell parameters: $\mathbf{a} = 14.206$ Å, $\mathbf{b} = 6.521$ Å, $\mathbf{c} = 7.403$ Å, $\beta = 90.08°$. From total energy calculations, this distorted system is slightly more stable than the classical β model with an energy stabilization of 0.06 eV/FU, and the calculations of Brown bond valences give reasonable values too: $Li^{I} = 0.99$ and $V^{III} = 2.94$. We can finally conclude that a distortion from a classical β unit cell is expected for $LiVOSO_4$ and we can also propose a distorted monoclinic unit cell (space group $P2_1/a$, $\mathbf{a}' = 2\mathbf{a}$) as a possible structure for this compound.

Finally, a comparison between experimental and simulated (with PowderCell software [58]) X-ray diffraction diagrams (Fig. 4) using the data of the monoclinic distortion shows that this model gives a quite good agreement in both positions and intensities. A few lines are however very broad on the experimental pattern but this was already the case for the non-intercalated compound and this may be due to a problem of stacking faults. Furthermore, a cell refinement based on the experimental pattern with the use of the optimized atomic coordinates as a structural constrain (Rietveld method) gave results which are very close to the optimized ones: $\mathbf{a} = 14.232$ Å, $\mathbf{b} = 6.456$ Å, $\mathbf{c} = 7.406$ Å, $\beta = 90.06°$. However, no clear evidence of a monoclinic distortion is obtained from this refinement due to the poor quality of the experimental data. A new structural investigation is in progress in order to confirm the unit cell (space group and values of the cell parameters) of $LiVOSO_4$, and to determine the exact order of the VO_6 and SO_4 polyhedra inside the cell.

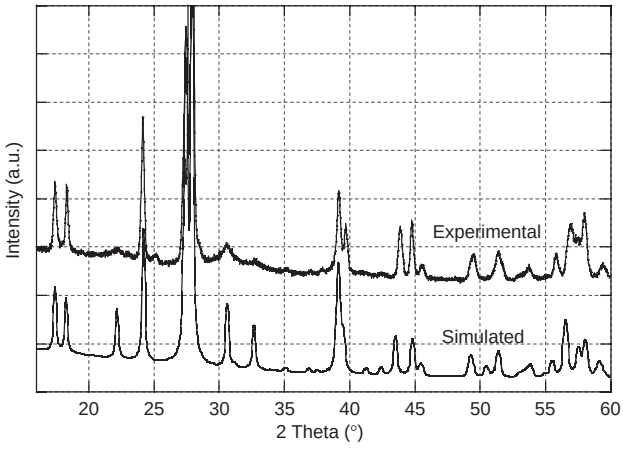

Fig. 4. Comparison of the X-ray diffraction diagrams for $LiVOSO_4$. The experimental diagram of Ref. [57] is shown at the top. The simulated pattern obtained by the PowderCell software [58] with the optimized cell for $LiVOSO_4$ is shown below. A pseudo-Voigt function with a classical Cagliotti variation is applied to simulate the experimental broadening.

5. Total energies and potential calculations

Table 5 gathers all the VASP total energies (per formula unit) of the relaxed systems and their corresponding calculated potentials, in both NSP and SP cases. The equilibrium voltage between negative and positive electrodes is defined as the difference of the lithium chemical potential between the two electrodes:

$$V(x) = \frac{\mu_{\mathrm{Li}}^{\mathrm{positive}}(x) - \mu_{\mathrm{Li}}^{\mathrm{negative}}}{zF}.$$

F is the Faraday constant, z is the charge (in electrons) transported by the lithium in the electrolyte. Using several approximations, Aydinol et al. [59] have shown that a good estimation of the mean potential can be obtained from total energy calculations. In our case, we have two-phases systems (Li_0VOXO_4, Li_1VOXO_4) and we use the following equation to determine the potential value:

$$V(x_1, x_2) = -\frac{[E_{\mathrm{tot}}(\mathrm{Li}_{x_2}\mathrm{VO}X\mathrm{O}_4) - E_{\mathrm{tot}}(\mathrm{Li}_{x_1}\mathrm{VO}X\mathrm{O}_4) - (x_2 - x_1)E_{\mathrm{tot}}(\mathrm{Li})]}{(x_2 - x_1)}$$

with $x_2 = 1$ and $x_1 = 0$.

In Table 5, we may observe a quite large difference between the calculated and experimental potentials (from 0.57 to 0.86 V). In the first paper of Aydinol et al. [59], a difference of about 0.4 V was found, and this difference was explained by an overestimation of the lithium cohesive energy. Other authors found such a difference when studying the V_2O_5 electrochemical behavior [3–5]. However, very recently, Morgan et al. [18] have reported the presence of systematic errors in the prediction of the potential ranging from 0.3 to 1.3 V, and no clear explanation has been given. To be sure that the choice of the method (PAW/plane wave) is not at the origin of this problem, we have also calculated the electrochemical potential using the total energy from the WIEN2K method. Results of both approaches are very similar (Table 5), and cannot explain the observed differences. Nevertheless, a larger underestimation of the potential (lower potential values) is observed when a "hetero-atom" X (P, As, S) is present. We have shown that X–O bonds are not well described, with a systematic overestimation of the bond lengths; as a consequence, Brown valences are underestimated: they are about 4.6–4.7 for both P^{V} and As^{V}, and 5.7–5.8 for S^{VI}. Finding a new exchange and correlation potential which better describes these bond lengths can be a challenge.

However, the estimated values of potentials are fully consistent with the other data from the literature and with our understanding of the inductive effect. The V^{V}/V^{IV} potential of the Li_xVOXO_4 ($X = P$, As) at about 3.15 V is intermediate between both calculated V^{V}/V^{IV} potentials of $Li_xV_2O_5$ (2.5 V) [5] and

Table 5
Total energies (eV/FU) and calculated potentials[a] (V) for the β–$VOXO_4$ compounds

X	$VOXO_4$ E_{tot}	$LiVOXO_4$ E_{tot}	VASP pot.[a]	WIEN2K pot.	Exp. pot. [30–32]
P	−54.896	−59.909 (*−59.621*)	3.12 (*2.83*)	3.14	3.98 (V^V/V^{IV})
As	−50.399	−55.460 (*−55.244*)	3.17 (*2.95*)	3.15	4.02 (V^V/V^{IV})
S	−49.798 (*−49.528*)	−53.962 (*−53.572*)	2.27 (*2.15*)	2.18	2.84 (V^{IV}/V^{III})

[a] Potentials were calculated by taking the total energy of bcc lithium obtained from a VASP calculation (−1.892 eV). In the case of both SP/NSP calculations, the NSP values are given in parentheses.

$Li_xV_2(PO_4)_3$ (3.3 V) [18]. In the same way, the V^{IV}/V^{III} potential of Li_xVOSO_4 (2.27 V) is found, as experimentally expected, below the V^{IV}/V^{III} potential calculated for $Li_xV_2(PO_4)_3$ (2.5 V) [18]. For the Li_xVOXO_4 compounds, a difference of about 1 V is also obtained between V^V/V^{IV} and V^{IV}/V^{III} potentials.

6. Band structure calculations: analysis and discussion

In order to better understand the behavior of the β-$VOXO_4$ compounds versus Li intercalation, we calculated their band structures using the WIEN2K/FLAPW method. The total densities of states (DOS) of the six compounds are presented in Fig. 5. For comparison, we also calculated the total DOS of γ-V_2O_5 and ζ-$Li_2V_2O_5$ [5]; ζ-$Li_2V_2O_5$ is obtained from γ-V_2O_5 by a simple topotactic reaction, corresponding to a V^V/V^{IV} change in the vanadium oxidation state. When using DFT, one critical point is the determination of an origin for the Kohn–Sham energies, also called band energies. In fact, the total energy is independent of this reference as a double counting correction is introduced. So, arbitrarily, the Fermi level is often chosen as the origin of the energy. Here we made a different choice in order to better discuss the evolution of the band structure. We have defined an energy origin for each $VOXO_4/LiVOXO_4$ system. For non-intercalated compounds, the zero energy was set at the top of anionic (oxygen p) band. We then considered that X atoms are not significantly affected by intercalation because there is no change in the X–O bond lengths. Consequently, the energy reference of the $LiVOXO_4$ compounds was shifted in order to impose the same energy as in $VOXO_4$ for the 1s orbital of a given X atom. All DOS of Fig. 5 are represented for one formula unit.

The total DOS of the V_2O_5/LiV_2O_5 system (top of Fig. 5) is clearly separated in two blocks. The low-energy part (the "p" band) mainly comes from the oxygen 2p states (shown in projection) and the upper part, called the "d" band, has a vanadium 3d dominant character. Due to the square pyramid environment for vanadium, the d band is split into three parts. For a better understanding, it is convenient to consider the square pyramid as a distorted octahedron with the z-axis

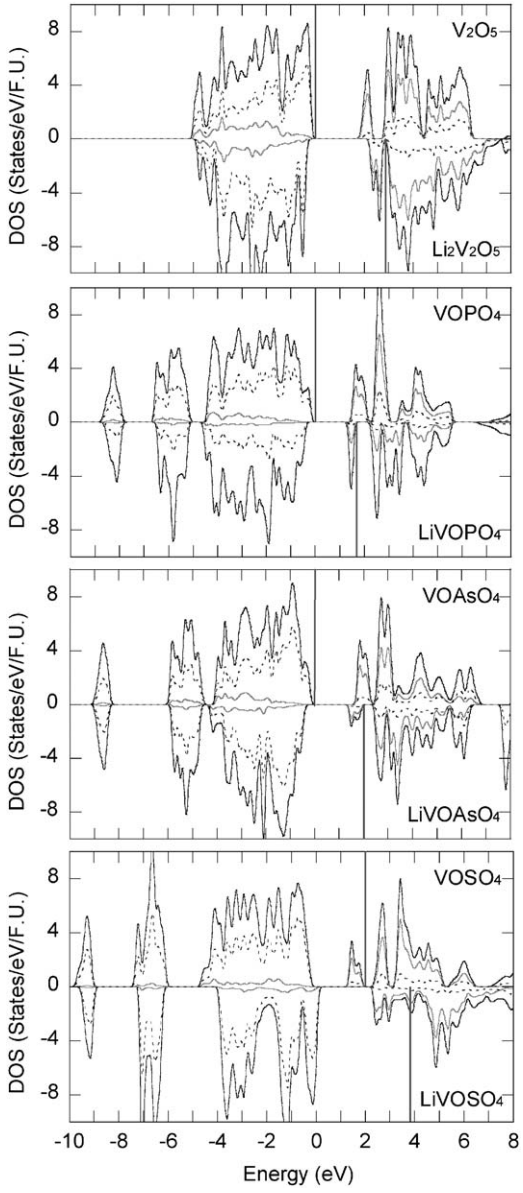

Fig. 5. Densities of states (DOS) of $V_2O_5/Li_2V_2O_5$ and $VOXO_4/Li_1VOXO_4$ (X = P, As, S). Fermi levels are represented by vertical lines. Solid black lines, solid grey lines and dashed black lines are used for total DOS, vanadium partial DOS and oxygen partial DOS, respectively.

along the vanadyl bond. The anti-bonding σ^* orbitals, $d_{x^2-y^2}$ and d_{z^2}, are found at the top of the d band. The intermediate block, corresponding to anti-bonding π^*

states, has d_{xz} and d_{yz} characters. Finally, the non-bonding d_{xy} orbital is found well separated, at the bottom of the d band. These states are non-bonding due to the off-centering of vanadium atom from the equatorial plane.

Before lithium intercalation into γ-V_2O_5, the vanadium oxidation state is V (d^0 configuration). Actually, no electron is found in the d band. However, the covalent mixing between vanadium and oxygen (see the metal d character into the p band) induces a population of the vanadium d orbitals that is far away from zero (1.825 electron) (Table 6). Upon lithium intercalation, the vanadium oxidation state tends to IV and a d^1 configuration is expected. In the band structure, one electron is added at the bottom of the d band. The entire d band moves up and a shrinking of the p band is visible. We may exclude that this displacement of the d band is due to a spurious effect of DFT calculations. Similar effects have been observed when lithium is intercalated in TiS_2 [60] or in $Li_xV_2O_5$ with, for the later, a gradual displacement of the d band as function of the intercalation rate [61]. Nevertheless, from Table 6, we can notice that the total charge on the d orbitals is only slightly modified, going from 1.825 for d^0 to 1.904 for d^1. The main point is the electron redistribution on the metal site. We observe a lower contribution of the d orbitals to the p band, corresponding to a more ionic V–O bond: 1.209 instead of 1.752, and a higher occupancy of the non-bonding orbital (by 0.649). As a matter of fact, for one electron added into the d band, only 65% are really found into the atomic sphere chosen for the calculations. The remaining part is mainly dispersed outside this sphere and is found into the interstitial part. As the V–O bond is more ionic in $Li_2V_2O_5$ than in V_2O_5, we will find more electronic density on the oxygen atoms for the former. This is what we can call a ''back transfer''.

We can find many similarities between all the electronic structures of the β-$VOXO_4$ systems: stabilization of the d_{xy} orbital at the bottom of the d band and an energy gap close to 2 eV between the p and the d bands. The main difference between the β-$VOXO_4$ compounds and V_2O_5 comes from the shape of the p band that is highly affected by the strong covalent X–O interactions. The p band is now divided into three parts, with two blocks below the ''classical'' p band, corresponding to the σ bonding X–O interactions: below -8 eV with a_1 symmetry, and between -8 and -4.5 eV with t_2 symmetry [62]. As a consequence, the width of the p band increases by 5 eV for V_2O_5, 9 eV for $VOPO_4$, and up to 10 eV for $VOSO_4$, which has the more covalent X–O interaction. A direct effect is a drastic change in the V–O interaction. The partial occupancy of the d orbitals in the p band is reduced from 1.752 to 1.722 and 1.728 for $VOPO_4$ and $VOAsO_4$, respectively, and the total occupancy of the d orbitals is also reduced (Table 6). This corresponds to a more ionic interaction of the oxygens with the vanadium in $VOPO_4$ and $VOAsO_4$ than in V_2O_5. This explains why the position of the d band is lower in energy in $VOPO_4$ and $VOAsO_4$ compared to V_2O_5: the smaller the occupancy of the d orbitals, the lower the energy of the states. Upon lithium intercalation, $LiVOPO_4$ and $LiVOAsO_4$ behave as $Li_2V_2O_5$, i.e. a shrinking of the p band and an increase of the ionicity for the V–O interaction are observed. We finally find a smaller total d charge for $LiVOPO_4$ and $LiVOAsO_4$ than for $Li_2V_2O_5$, and, therefore, lower d band and Fermi level. All these points are in favor of an increase of the V^V/V^{IV} electrochemical potentials from $Li_2V_2O_5$ to $LiVOPO_4$ and $LiVOAsO_4$. Note that in the whole study, the very close electronegativities of P and As atoms is confirmed by a very similar behavior.

For the $VOSO_4/LiVOSO_4$ system, a higher covalent character is expected for the SO_4 tetrahedron due to the closer electronegativity of sulfur and oxygen atoms ($\chi_P = 2.1$, $\chi_{As} = 2.0$, $\chi_S = 2.5$ and $\chi_O = 3.5$, according to Pauling electronegativity scale). The induced more ionic V–O interaction is reflected by the partial DOS of vanadium in the p band (Fig. 5). In this way, one can understand that the potential of V^{IV}/V^{III} for $VOSO_4/LiVOSO_4$ (experimentally 2.84 V) is much higher than the one of V^{IV}/V^{III} for the V_2O_5 system (2.2 V) where no inductive effect is present [5]. As a consequence, this potential is found very close to the V^V/V^{IV} potential of the V_2O_5 system.

Our main conclusion is that for a given oxidation number, the more ionic the V–O interaction, the higher the electrochemical potential. We have also shown that we can deeper understand the inductive effect by a quantitative analysis of the electronic band structure calculations. For a different representation of the evolution of the V–O interaction we have plotted in Fig. 6 the partial atomic DOS for the X, V and O atoms divided by the total DOS. As ''fat bands'' do for band structures, this ''*relative projected DOS*'' representation allows an easy visualization of each atomic contribution as a function of the energy, whatever the DOS shape: sharp peak or broad band. It has been used for the first time in Ref. [63]. For all the energy range, a pure atomic state (the extreme case for ionic interaction) gives a

Table 6
Partial and total occupancies of vanadium d orbitals for different energy bands

	s Band	p Band	d Band	Total
V_2O_5	0.073	1.752		1.825
$Li_2V_2O_5$	0.046	1.209	0.649	1.904
$VOPO_4$	0.056	1.722		1.778
$LiVOPO_4$	0.035	1.213	0.628	1.876
$VOAsO_4$	0.059	1.728		1.787
$LiVOAsO_4$	0.037	1.223	0.620	1.880
$VOSO_4$	0.034	1.216	0.626	1.876
$LiVOSO_4$	0.018	0.703	1.279	2.000

value close to 100% and, on the contrary, a highly covalent interaction induces a number close to 50%. The evolution from a rather covalent V–O interaction in V_2O_5 to a very ionic one in Li_1VOSO_4 is clearly shown by the evolution of the vanadium contribution in the p block between -5 and 0 eV. Concerning the X–O interaction (-10 to -8 eV), we find, as expected, the higher X character in the p states at lower energy and the counterpart of this σ interaction is clearly visible above the d band.

Now, we will present a model that can help to better understand the origin of the electrochemical potential obtained from band structure calculations. Solid-state chemists are more used to discuss in terms of band structures and energy levels instead of total energies. For this reason, the expression that gives the potential as a function of the total energies of three compounds does not help too much. In order to build our model, we will assume that if we define a correct and unique reference for the band energies of the systems under study, we will be able to interpret the difference observed for the total energy by a difference between the Kohn–Sham energies of the valence states for the three systems. This gives $\Delta E_{tot} \approx \Delta E_{KS}$, neglecting variations of other terms (see p. 82 of Ref. [49] for details about the expression of the total energy).

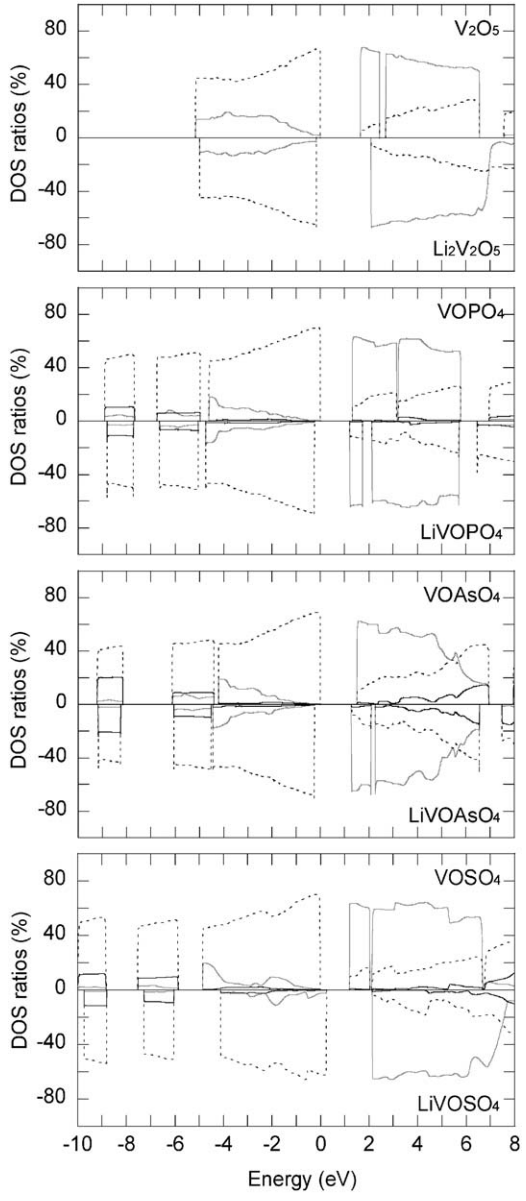

Fig. 6. Ratio (in %) of partial DOS to total DOS for atomic V, X and O contributions in solid grey lines, solid black lines and dashed black lines, respectively. The contribution of the interstitial part is not shown.

By this way, the equation giving the potential now becomes

$$V = -[E_{KS}(LiVOXO_4) - E_{KS}(VOXO_4) - E_{KS}(Li)]$$

$$\text{with } E_{KS} = \int^{E_F} E\,DOS(E)\,dE$$

and the potential can be obtained by the difference between $\int^{E_F} E\,DOS(E)\,dE$ of two systems having exactly the same number of electrons: a real one corresponding to $LiVOXO_4$, and a fictive one built by the sum of the DOS for the occupied states of $VOXO_4 \oplus Li$.

$$V = -[E_{KS}(LiVOXO_4) - E_{KS}(VOXO_4 \oplus Li)].$$

As the energy reference between $LiVOXO_4$ and $VOXO_4$ is imposed by using the 1s level of the X atom, we just had to optimize the position of the lithium band energy scale in order to verify $\Delta E_{KS} = \Delta E_{tot}$. This ΔE_{tot} value has been calculated at 3.15 eV (Table 5) in the case of $LiVOAsO_4/VOAsO_4$. Superposition of the $LiVOAsO_4$ and $VOAsO_4 \oplus Li$ DOS (Fig. 7 top) allows to show a schematic illustration of the band evolution during the intercalation (Fig. 7 bottom). However, this figure can be used for the interpretation of the potential only if we are not too far from a rigid band model. So, in order to interpret the physical origin of the calculated potential, we plotted the evolution of the difference between the band energy $\Delta E_{KS}(n)$ with $E_{KS}(n) = \int^n E(n)\,dn$ as a function of the number of valence electrons (Fig. 8).

The interpretation of the ΔE variation is clear if we consider the displacement of the different bands of Fig. 7. We observe no contribution from the arsenic 3d band (between 10 and 20 electrons), which reinforces our choice of energy reference. From this representation, it is clear that the system nearly behaves as a perfect rigid band model, because the energy difference is very close to zero (0.2 eV) before adding the last electron. Thus, 90% of the final stabilization directly comes from the charge transfer from the lithium 2s orbital to the d band.

Coming back to Fig. 7, and if we consider that only the last electron contributes to the potential, the 3.15 V value can be obtained by the transfer of one electron

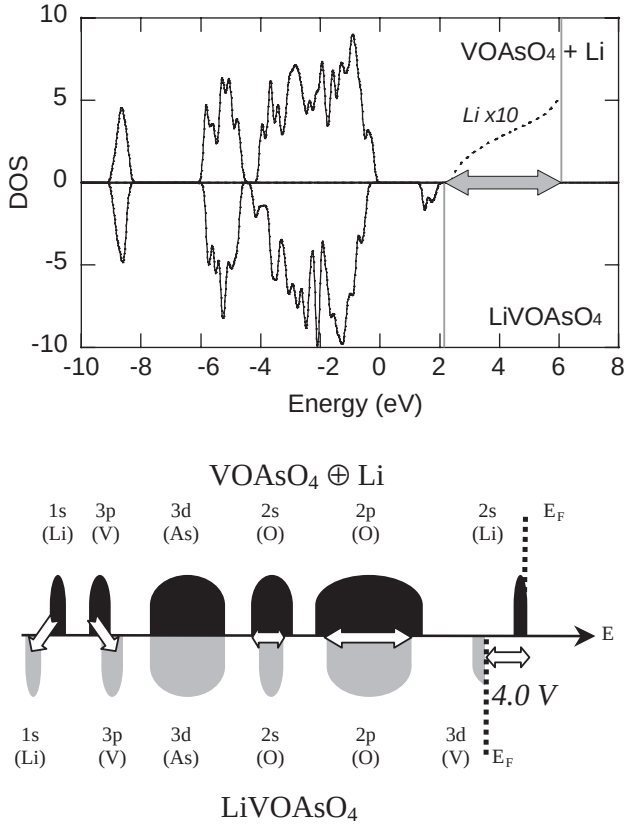

Fig. 7. Top: calculated DOS for both $VOAsO_4 \oplus Li$ (Li DOS in dashed lines) and $LiVOAsO_4$ systems. Bottom: schematic illustration of the DOS obtained for $VOAsO_4 \oplus Li$ and $LiVOAsO_4$ systems. DOS are truncated at the Fermi levels.

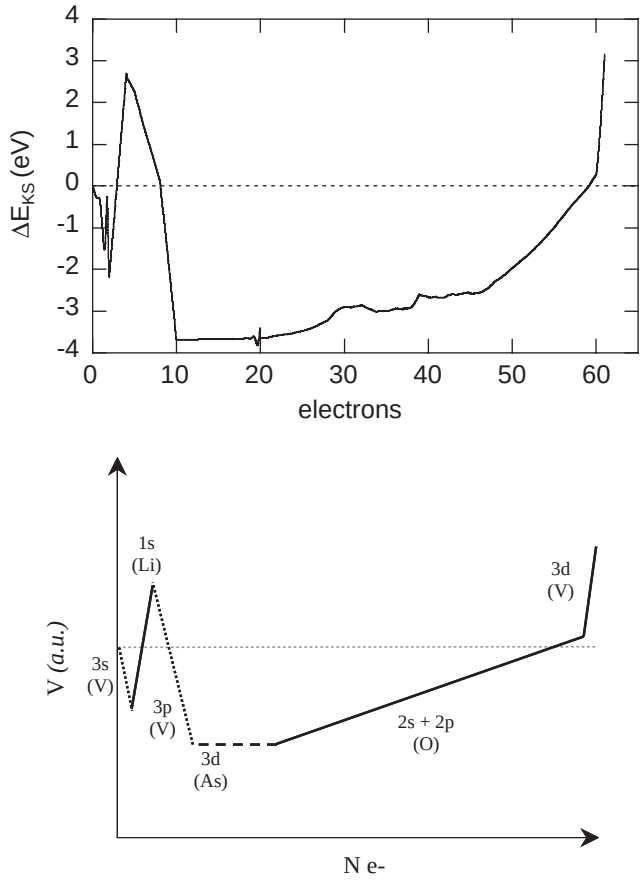

Fig. 8. Calculated (upper part) and schematic (lower part) evolutions of the potential as a function of the number of valence electrons for the "$Li \oplus VOXO_4$"/$LiVOXO_4$ system.

from the center of gravity of the occupied Li 2*s* orbital to the bottom of the vanadium *d* band. If the *d* band is stabilized by inductive effect, a higher potential is expected and if the *d* band moves up due to a reduction of the cation, a decreasing of the potential is observed. A more classical way to represent a battery potential in a rigid band model is to consider the difference between the highest occupied point of the lithium DOS for the "$VOAsO_4 \oplus Li$" and the highest occupied vanadium 3*d* orbitals of $LiVOAsO_4$. We get in this case a larger value of 4.0 V because we consider now only the Fermi level of metallic lithium, instead of the integration on the entire 2*s* lithium band. By doing so, we are much closer to the experiment, in which the potential of lithium is considered as constant (reference electrode).

7. Conclusion

In this work, we studied three β-Li_xVOXO_4 compounds ($x = 0$, 1 and $X = P$, As, S). We performed some DFT calculations for geometry optimizations that have given reliable results for parameters and Li–O and V–O and validated our proposed models for $VOAsO_4$ and $LiVOSO_4$ according to Brown valences results. Total energy calculations gave reasonable values for the potentials compared to the experimental ones but still with some discrepancies that are not fully explained yet. An analysis of band structure calculations led to a comparison of DOS with the $Li_xV_2O_5$ systems, showing the role played by the strongly covalent *X*–O interaction on the V–O interactions. By working with two systems (real $LiVOXO_4$ and fictive $Li \oplus VOXO_4$) we could finally propose a model that helps to understand the origin of potentials from band structure analysis instead of total energies differences.

Acknowledgments

The authors thank J. Gaubicher for general discussions and providing the XRD diagrams of $LiVOSO_4$. They also thank the CINES (Centre Informatique National de l'Enseignement Supérieur, Montpellier, France) for allowing the use of SGI supercomputer in order to perform these calculations.

References

[1] C. Delmas, H. Cognac-Auradou, J.M. Cocciantelli, M. Ménétrier, J.P. Doumerc, Solid State Ionics 69 (1994) 257 and references therein.
[2] J. Galy, J. Solid State Chem. 100 (1992) 229 and references therein.
[3] J.S. Braithwaite, C.R.A. Catlow, J.D. Gale, J.H. Harding, Chem. Mater. 11 (1999) 1990.
[4] J.S. Braithwaite, C.R.A. Catlow, J.D. Gale, J.H. Harding, P.E. Ngoepe, J. Mater. Chem. 10 (2000) 239.
[5] X. Rocquefelte, F. Boucher, P. Gressier, G. Ouvrard, Chem. Mater. 15 (2003) 1812.
[6] J. Gopalakrishnan, K. Kasturirangan, Chem. Mater. 4 (1992) 745.
[7] K.S. Nanjundaswamy, A.K. Padhi, J.B. Goodenough, S. Okada, H. Ohtsuka, H. Arai, J. Yamaki, Solid State Ionics 92 (1996) 1.
[8] A.K. Padhi, K.S. Nanjundaswamy, C. Masquelier, J.B. Goodenough, J. Electrochem. Soc. 144 (1997) 2581.
[9] G.B.M. Vaughan, J. Gaubicher, T. Le Mercier, J. Angenault, M. Quarton, Y. Chabre, J. Mater. Chem. 9 (1999) 2809.
[10] H. Ohkawa, K. Yoshida, M. Saito, K. Uematsu, K. Toda, M. Sato, Chem. Lett. 28 (1999) 1017.
[11] J. Gaubicher, C. Wurm, G. Goward, C. Masquelier, L. Nazar, Chem. Mater. 12 (2000) 3240.
[12] B.L. Cushing, J.B. Goodenough, J. Solid State Chem. 162 (2001) 176.
[13] R. Benedek, M.M. Thackeray, L.H. Yang, Phys. Rev. B 56 (1997) 10707.
[14] R. Benedek, M.M. Thackeray, L.H. Yang, J. Power Sources 81–82 (1999) 487.
[15] J.B. Goodenough, H.Y.P. Hong, J.A. Kafalas, Mater. Res. Bull. 11 (1976) 203.
[16] L.O. Hagman, P. Kierkegaard, Acta Chem. Scand. 22 (1968) 1822.
[17] A.K. Padhi, Mapping Redox Energies of Electrode Materials for Lithium Batteries, Ph.D. Thesis, University of Texas, Austin, 1997.
[18] D. Morgan, G. Ceder, M.Y. Saïdi, J. Barker, J. Swoyer, H. Huang, G. Adamson, Chem. Mater. 14 (2002) 4684.
[19] A. Manthiram, J.B. Goodenough, J. Power Sources 26 (1989) 403.
[20] R. Gopal, C. Calvo, J. Solid State Chem. 5 (1972) 432.
[21] B. Jordan, C. Calvo, Can. J. Chem. 51 (1973) 2621.
[22] S. Boghosian, K.M. Eriksen, R. Fehrmann, K. Nielsen, Acta Chem. Scand. 49 (1995) 703.
[23] H.R. Tietze, Aust. J. Chem. 34 (1981) 2035.
[24] D. Beltran-Porter, A. Beltran-Porter, P. Amoros, R. Ibañez, E. Martinez, A. Le Bail, G. Ferey, G. Villeneuve, Eur. J. Solid State Inorg. Chem. 28 (1991) 131.
[25] F. Benabdelouahab, J.C. Volta, R. Olier, J. Catal. 148 (1994) 334.
[26] A. Chauvel, M.E. De Roy, J.P. Besse, A. Benarbia, A. Legrouri, A. Barroug, Mater. Chem. Phys. 40 (1995) 207.
[27] S. Boudin, A. Guesdon, A. Leclaire, M.M. Borel, Int. J. Inorg. Mater. 2 (2000) 561.
[28] P.Y. Zavalij, M.S. Whittingham, Acta Crystallogr. B 55 (1999) 627.
[29] M. Schindler, F.C. Hawthorne, W.H. Baur, Chem. Mater. 12 (2000) 1248.
[30] J. Gaubicher, T. Le Mercier, Y. Chabre, J. Angenault, M. Quarton, J. Electrochem. Soc. 146 (1999) 4375.
[31] J. Gaubicher, F. Orsini, T. Le Mercier, S. Llorente, A. Villesuzanne, J. Angenault, M. Quarton, J. Solid State Chem. 150 (2000) 250.
[32] J. Gaubicher, Y. Chabre, J. Angenault, A. Lautié, M. Quarton, J. Alloys Comp. 262–263 (1997) 34.
[33] G. Kresse, J. Hafner, J. Phys. Condens. Mater. 6 (1994) 8245.
[34] G. Kresse, J. Hafner, Phys. Rev. B 49 (1994) 14251.
[35] G. Kresse, J. Furthmüller, Comput. Mater. Sci. 6 (1996) 15.
[36] G. Kresse, J. Furthmüller, Phys. Rev. B 54 (1996) 11169.
[37] P.E. Blöchl, Phys. Rev. B 50 (1994) 17953.
[38] G. Kresse, D. Joubert, Phys. Rev. B 59 (1999) 1758.
[39] D. Vanderbilt, Phys. Rev. B 41 (1990) 7892.
[40] J.P. Perdew, in: P. Ziesche, H. Eschrig (Eds.), Electronic Structure of Solids, Akademie Verlag, Berlin, 1991.
[41] J.P. Perdew, K. Burke, Y. Wang, Phys. Rev. B 54 (1996) 16533.
[42] P.E. Blöchl, O. Jepsen, O.K. Andersen, Phys. Rev. B 49 (1994) 16223.
[43] H.J. Monkhorst, J.D. Pack, Phys. Rev. B 13 (1976) 5188.
[44] R.P. Feynman, Phys. Rev. 56 (1939) 340.
[45] K.H. Lii, C.H. Li, C.Y. Cheng, S.L. Wang, J. Solid State Chem. 95 (1991) 352.
[46] J.M. Longo, R.J. Arnott, J. Solid State Chem. 1 (1970) 394.
[47] P. Blaha, K. Schwarz, G.K.H. Madsen, D. Kvasnicka, J. Luitz, WIEN2K: an augmented plane-wave + local orbitals program for calculating crystal properties, ISBN 3-9501031-1-2.
[48] K. Schwarz, P. Blaha, G.K.H. Madsen, Comput. Phys. Comm. 147 (2002) 71.
[49] D.J. Singh, Plane Waves, Pseudopotentials and the LAPW Method, Kluwer Academic Publishers, Dordrecht, 1994.
[50] I.D. Brown, Acta Crystallogr. B 48 (1992) 553.
[51] V.M. Goldschmidt, Skr. Nor. Vidensk. Akad. Oslo 8 (1927) 7.
[52] L. Pauling, J. Am. Chem. Soc. 51 (1929) 1010.
[53] L. Pauling, J. Am. Chem. Soc. 69 (1947) 542.
[54] W.H. Zachariasen, J. Less-Common Met. 62 (1978) 1.
[55] I.D. Brown, D. Altermatt, Acta Crystallogr. B 41 (1985) 244.
[56] N.E. Brese, M. O'Keeffe, Acta Crystallogr. B 47 (1991) 192.
[57] J. Gaubicher, Nouveaux matériaux d'électrode positive pour batteries au Lithium, Ph.D. Thesis, Paris VI, France, 1998.
[58] W. Kraus, G. Nolze, PowderCell for Windows Version 2.3, Berlin, Germany, 1999.
[59] M.K. Aydinol, A.F. Kohan, G. Ceder, K. Cho, J. Joannopoulos, Phys. Rev. B 56 (1997) 1354.
[60] C. Umrigar, D.E. Ellis, D. Wang, H. Krakauer, M. Posternak, Phys. Rev. B 26 (1982) 4935.
[61] X. Rocquefelte, Modélisation du comportement électrochimique de matériaux pour batteries au lithium à partir de calculs de premiers principes, Ph.D. Thesis, Nantes, 2001.
[62] S.F.A. Kettle, Physical Inorganic Chemistry. A Coordination Chemistry Approach, Oxford University Press, Oxford, 1996.
[63] F. Boucher, Z. Zhukov, M. Evain, Inorg. Chem. 35 (1996) 7649.